CrossMark

Case microstructure in induction surface hardening of steels: an overview

Umberto Prisco[1]

Abstract
The microstructure and resultant mechanical properties of the hardened case produced in steels by induction surface hardening are discussed. The development of the final structure is followed throughout its characteristic evolutionary stages; its dependence on heating and cooling rate, maximum temperature of the treatment, composition, and initial microstructure is described in detail. Gradients of microstructure, composition, and hardness brought about by induction surface hardening inside the case are studied and explanations about their origin are proposed. The properties of the hardened case completely rely upon its microstructure, whose control is then a key factor for engineering applications.

Keywords Induction surface hardening · Steel · Hardened case · Microstructure · Austenite · Martensite

1 Introduction

Induction heat hardening has become increasingly important through the last decades [1, 2]. The advantages of induction heat treatments over the traditional methods are numerous: short treatment time, repeatability, high efficiency with consequent energy savings, no naked flame or atmosphere safety issues, rapid focused heat, and increased automation of the process. Some of these features make induction heating ecologically more favorable than conventional furnace-based heat treatments [3].

In particular, induction surface hardening, as technique applied to steels, is receiving increased attention by the industrial and scientific world. With this technique, a hardened surface layer, called hardened case, can be formed with a depth ranging from sub-millimeter to a few millimeters. This technique allows to selectively harden surfaces without affecting the interior structure of the part.

The increasing use of surface-hardened steels for many industrial components, e.g., gears, bearings, shafts, and cut-

ting tools, coupled with the use of complex monolithic components in the manufacturing industry, has lately brought a spread of induction hardening techniques [4, 5]. For example, because of the need of performing treatment over complex surfaces, the spot induction hardening has been developed. This technique adopts a single-turn copper coil coupled to a five-axis CNC machine tool to realize a small region heat treatment of curved surface or some other complicated shapes [1, 6, 7].

The automotive industry has played a decisive role in bringing new attention on induction surface hardening due to its need to achieve weight reduction of the vehicle structures without compromising passengers' safety. In this field, the interest about induction treatments is also linked to the push to develop innovative heat treatment procedures that can be used as an alternative to the current production methods for advanced steels [8].

During induction hardening, the metal undergoes a double phase-transformation, first to austenite, upon heating, and then, upon quenching, to martensite, so that the hardness of the part increases. Besides the main phase-transformations, many other phenomena, as recrystallization, grain growth, carbide dissolution, and diffusion of alloying elements, can be involved in the process. Many technological parameters, such as the form of the induction coil, its distance from the surface, current frequency, current, and moving rate of the induction coil, can affect the microstructure and properties of the treated part. Thus, it is possible to state that induction

✉ Umberto Prisco
umberto.prisco@unina.it

[1] Department of Chemical, Materials and Production Engineering, University of Napoli Federico II, Piazzale Tecchio 80, 80125 Naples, Italy

🍂 Springer

hardening is one of the most complex from a metallurgical point of view among the heat treatments.

Induction surface hardening is even more complex because the aforementioned phase transformations happen in the thin superficial layer of the workpiece. The rapid heating and cooling of the process generate sharply different thermal cycles in function of the depth below the surface. This results in a gradient of microstructure and proprieties within the hardened case. Evaluation of the case depth and its microstructure is important for controlling the quality of the components and to guarantee the fulfillment of the required mechanical performances [3, 9–12].

The hardened case can be defined in two different ways. The effective case is the layer under the surface showing a hardness higher than a specific level (frequently, it is the depth below the surface measured to 40 HRC); the total case is the layer under the surface showing differences in microstructural properties as compared to the core [13]. The total case is deeper than the effective case; therefore, their difference defines a case-core transition zone, or just transition zone, which can be very important for part performance.

To study the case microstructure, a three-step approach is needed. In the first step, the thermal cycle generated by the process is discussed, in the second step the post-heating microstructure is described, and then in the last step the alterations of the microstructure caused by the quenching are highlighted.

2 Thermal cycles inside the workpiece

The heating mechanism during induction heating is due to two phenomena. The principal one, active for any material which presents electrical resistivity, is the Joule heating due to the induced eddy current. The magnetic field produced by the alternating current circulating in the induction coil induces eddy currents in the workpiece. The eddy currents have the same frequency and opposed verse to the coil current. The resultant distribution of heating power density inside the workpiece is function of the electromagnetic coupling between the coil and workpiece. The second mechanism, occurring only for ferromagnetic materials, is caused by the energy dissipation required to reverse the magnetic domains inside the workpiece, the so-called magnetic hysteresis. This mechanism is active only below the Curie temperature, Ac_2, 768 °C for Fe-C, because the relative permeability of the steel, the main factor of the magnetic energy losses, drops to values around 1 approaching the Curie temperature. Compared with the magnetic losses, the Joule effect has a much greater influence on the overall heating throughout the process, in particular above the Curie temperature [14].

The distribution of the eddy currents within the workpiece perpendicularly to its surface is not uniform; the current density decreases from the surface toward the workpiece core. Indeed, the highest values of the eddy currents are mainly produced close to the surface of the workpiece in what is often referred to as "skin effect." This means that almost all of the heat is produced near the surface. For practical purposes, to describe this phenomenon, a current penetration depth or skin depth, δ, is used [15]. Under the assumption of an exponential decay of the eddy current density, and then of the heating power density, from the surface toward the workpiece core, δ is defined as the distance from the surface, at which the current decreases to $1/e$ its surface value. Then, the power density at this distance is equal to $1/e^2$ its value at the surface. Using this approximation, the skin depth can be calculated as $\delta = 503\sqrt{\rho/(\mu_r F)}$, where F is the frequency (Hz) of the inducing current, ρ is the electrical resistivity (Ωm), and μ_r is the relative magnetic permeability of the workpiece. It can be demonstrated that the skin depth is the layer within which the 86% of all the power induced is concentrated while, at a depth equal to the skin depth, the current is 37% of its surface value.

However, the assumption of exponential decay of the current density is correct only for a material having constant electrical resistivity and magnetic permeability and can be very misleading in the case of surface hardening. The codependence of permeability, resistivity, specific heat, and temperature, coupled with the non-standard behavior of steel near the Curie point, see Fig. 1 for example, is the cause of many difficulties in the study of the evolution of the heating power density profile during induction heating.

The process develops in three stages (see Fig. 2). First, in the cold stage, the power density and the heat rate increase very steeply, because the material heats up both for the Joule and magnetic losses. The surface material, being the one more coupled to the magnetic flow, is the main site of the heating in this stage. For this reason, the surface layer temperature will approach Ac_2 before the deeper layers. When the temperature in the surface layer rises above Ac_2 its permeability falls to 1, stopping the magnetic losses in this layer. As consequence, the rate of heat production falls in comparison with the deeper layers whose temperature is still under Ac_2. This, in association with the spike of the specific heat and with the increase in heat dissipation due to the rise in temperature, reduces the heating rate of the surface layer. A further lowering of the heating rate is due to the heat absorption of the on-heating phase transformation to austenite which starts at temperature around 720 °C.

This lowering of the heating rate produces a typical temperature-time profile with a double slope: a steep heating rate in the first part followed by a more gentle one so that the average heating rates used in the industrial practise, ranging from ~ 100 to 1000 °C/s, are reduced to a much lower value in the temperature range of the transformation, i.e., above
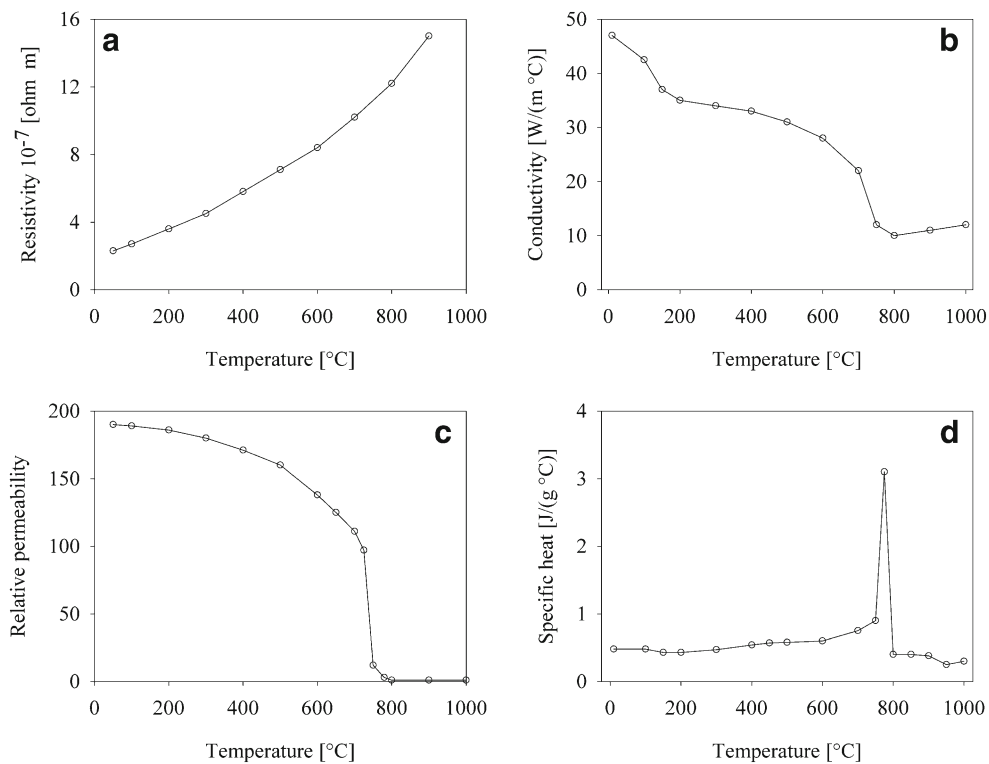
Fig. 1 **a** Electrical resistivity, **b** conductivity, **c** relative permeability, and **d** specific heat of the 55CrMo steel. Source: Li et al.[10]

720 °C. For example, in Fig. 3, to a nominal heating rate of 600 °C/s corresponds a real heating rate in the transformation zone of 270 °C/s.

The second stage of the process, called transition stage, starts when the surface temperature rises above Ac_2. The power density distribution along the thickness shows in this stage a typical wave shape, very different from the commonly assumed exponential distribution; in literature, this is called the magnetic wave phenomenon [13, 16]. This shape presents two peaks: one at the workpiece surface and one at a determined distance from the surface, whence it starts again decreasing; owing to this phenomenon, the maximum of the power density can occur on an internal layer and not at the workpiece surface under certain conditions. The depth of the inner peak is not constant but increases with the passing of the time, as deeper and deeper layers reach Ac_2.
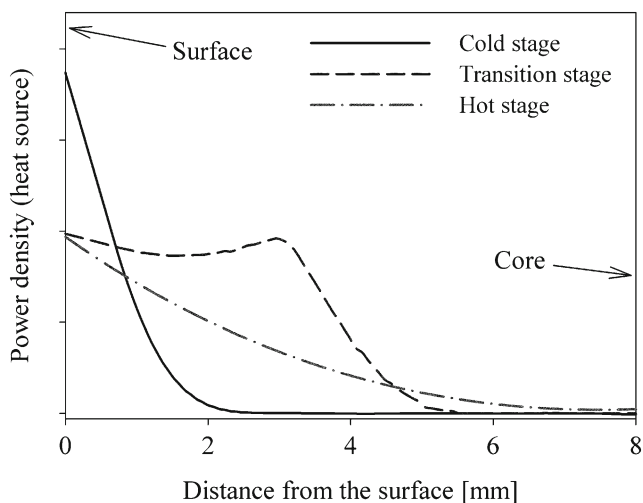
Fig. 2 Qualitative profiles of power density at different stages of induction heating of a steel bar. Redrawn after [13, 16]
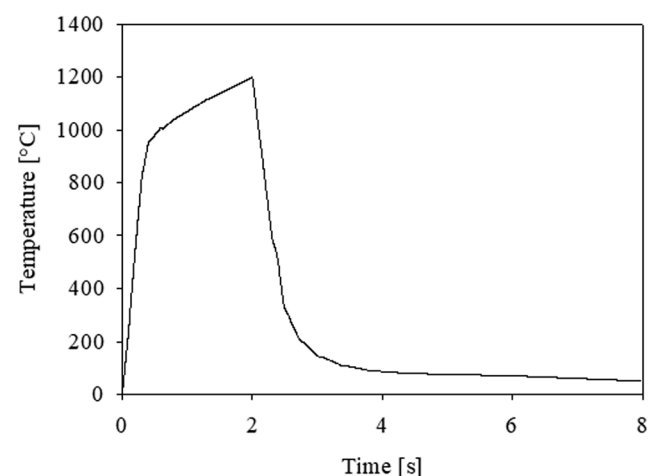
Fig. 3 Typical temperature-time profile at the workpiece surface for an induction surface hardening heat treatment

As soon as the whole workpiece has exceeded Ac_2, the last stage, the hot stage, starts and the profile of the power density returns to a classical distribution characterized by a smooth decrease from the surface to the core.

Obviously, in applications such as through hardening or induction heating, the transition stage is an insignificant portion of the induction process, due to the fact that the hot stage covers around 65% of the whole heating time. On the contrary, in induction surface hardening, the magnetic-wave phenomenon can be very significant in determining the temperature profile that develops within the workpiece. For example, a plateau on the temperature profile located near the surface can come about after the surface has reached Ac_2, especially for low power density applications. Under certain conditions, an inversion of the expected radial temperature profile during the heating up is observed, with the subsurface temperature being higher than the surface one [17]. While this inversion is quite uncommon, it can happen or for large case depth (≥ 20 mm) or for the use of inadequate process parameters or for the presence of high unexpected surface heat losses.

In the quenching stage, as expected, the surface region cools faster than the core. As consequence, after the quenching has started, the temperature profile shows higher temperatures inside the workpiece and not at the surface; subsurface regions might spend longer time at high temperatures, i.e., above Ac_3 or Ac_1, than the surface layer (this phenomenon can be additionally increases by the magnetic-wave phenomenon). Furthermore, the heat accumulated in the interior can temper back the superficial martensite if the quenching stage is stopped too early. All these phenomena have an enormous impact over the final microstructure of the hardened case, for example in term of the differential grain growth and nucleation over the distance below the surface.

Some possible evolutions of the temperature profile in the workpiece are reported in Fig. 4. Figure 4a shows the typical progress of the profile temperature during an induction surface hardening. There is first a sharp increase of temperatures with the surface being distinctly always at the highest temperature; during the earliest instants of the quenching stage, an internal maximum in the temperature profile shows up. In the case of Fig. 4b, the magnetic-wave phenomenon gives rise to a slight temperature maximum in the subsurface during the final part of the heating.

## 3 Microstructure evolution during the heating stage

Understanding phase transformation kinetics during the heating stage is a key point in the induction surface hardening of steels. Indeed, the austenite phase fraction, microstructure, and composition obtained during this stage play a major part in establishing the final microstructure and mechanical properties of the hardened case, considering that all on-cooling transformation products derive from the austenite generate in this phase. Moreover, it is of great importance to know how profiles of microstructures, for example in terms of grain size, concentration, and product phase fraction, are related to the distance from the surface.

It is well established that the kinetics of austenitization depends strongly upon the steel composition as well as the starting microstructure, more specifically distribution, size, and type of the starting phases. Any prior mechanical process that alters the microstructure is expected to heavily influence the austenitization kinetics. Moreover, this kinetics is strongly dependent from the heating rate, which is quite important in induction hardening applications.

The discussion about austenitization can be divided in two cases depending on the starting microstructure: ferrite-pearlite/pearlite (e.g., hypoeutectoid or eutectoid steel in hot-rolled or normalized conditions) and ferrite matrix with a dispersion of carbide/cementite particles (e.g., quenched and tempered steels or spheroidized steels obtained from a microstructure containing pearlite). According to the standard convention, the on-heating transformation temperatures are indicated by Ac with a subscript referring to the transformation type (Ae indicates the same temperatures at equilibrium condition). The following simple nomenclature will be herein adopted. For hypoeutectoid steels, Ac_1 is the temperature at which austenite begins to be experimentally observed and Ac_3 the temperature at which the austenitization is mainly completed; in case, some cementite is retained after Ac_3, as sometimes observed for a spheroidized pearlite microstructure, Ac_c indicates the temperature at which the solution of carbides in austenite is completed. Considering that for this class of steel the austenitization of pearlite is usually quite faster than that of proeutectoid ferrite (see below), many authors prefer to introduce beside Ac_1, the austenite start temperature, a pearlite to austenite transformation finish temperature; however, for the sake of simplicity, this nomenclature is not herein adopted. For hypereutectoid steel, Ac_1 is the temperature at which austenite begins to form and Ac_{fl} the temperature at which the transformation of ferrite to austenite is completed; at Ac_{fl}, some of the cementite/carbide has been dissolved to form austenite and some fraction of cementite is retained, so that for these steels there is always the need of introducing Ac_c with the abovementioned meaning.

Experimental studies pointed out that the austenite formation is a very complex phenomenon. The nucleation and growth of austenite begin from different sites in the initial microstructures which are characterized by different phases of different stability. However, previous researches showed
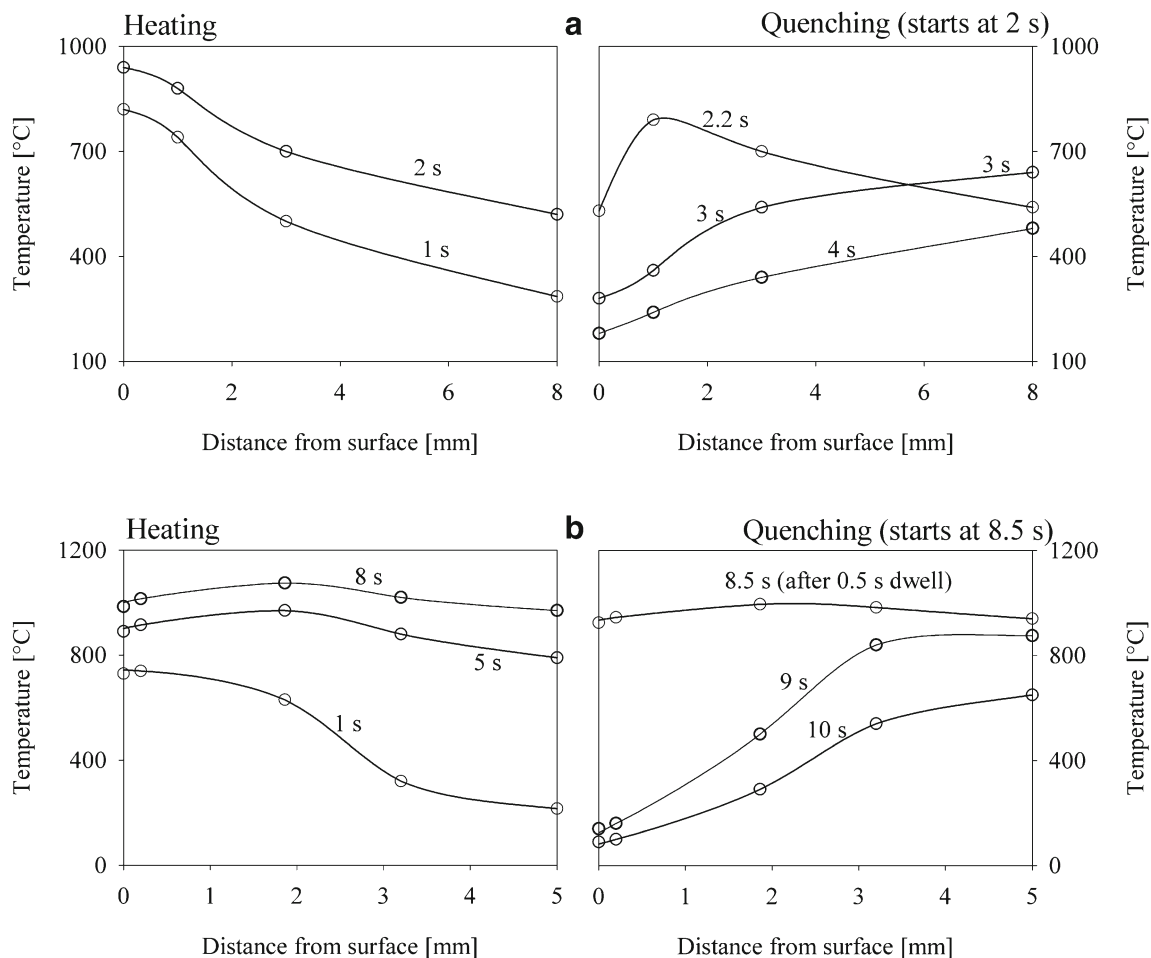
Fig. 4 Evolution of the temperature profiles during induction hardening. **a** Surface hardening of a 16-mm-diameter steel shaft (SAE 4340, 125 kHz; heating, 2 s). Redrawn after [13]. **b** Surface hardening of a 50-mm-diameter steel bar (SAE 1045, 10 kHz; heating, 8 s; dwell, 0.5 s) redrawn after [18]

that, as general rule, the pearlite-to-austenite transformation is much faster than the ferrite-to-austenite transformation [19–23]. The difference in the diffusion distances that atoms, especially carbon atoms, have to cover in the two cases is certainly the explanation. Indeed, diffusion distances are significantly shorter in lamellar pearlite, even in coarse pearlite, in comparison to proeutectoid ferrite, leading to high rates of pearlite dissolution. The dissolution of particles of cementite and other carbide is the slowest of all the concerned processes [24, 25].

3.1 Ferrite/pearlite mixtures

For a ferrite/pearlite microstructure, once Ac_1 has been reached, the pearlite is the first to start transforming into austenite. In particular, the austenitization begins from the pearlitic ferrite and continues into the pearlitic cementite. It was observed that pearlitic ferrite transforms to austenite very quickly compared to the pearlitic cementite, which dissolves in austenite at a slower rate [24, 26]. This two-step process of

austenitization of pearlite was observed to occur at high heating rate (higher than 20 °C/s), right in the heating rate range of interest for induction hardening, while at lower heating rates, ferrite and cementite plates seem to transform simultaneously [27].

The start of the transformation of the proeutectoid ferrite is the subsequent phase of the austenitization process. There is no agreement among the experimental observations of different authors whether the austenitization of pearlite and ferrite processes overlap or happen sequentially. Dykhuizen et al. [28] asserted that the conversion of the ferrite to austenite does not initiate until the pearlite region is one-tenth transformed to austenite because the ferrite cannot transform near Ac_1 until carbon is available from the pearlite region. In fact, if the transformation of ferrite is modeled as simultaneous with the transformation of the pearlite the resulting forecast fits poorly with the experimental data. Savran et al. [21] and Jayaswal et al. [29] also support the idea of a probable overlapping of pearlite-to-austenite and ferrite-to-austenite transformations while proposing different explanation of the phenomenon.

On the contrary, other researchers are in favor of the strict sequentiality of the two stages: first the dissolution of the pearlite then the transformation of the proeutectoid ferrite. To this regards, see, for example, Katsamas [26], Puskar [30], and Schmidt et al. [31] or Garcia de Andres et al. [32] in their study of austenitization in DP steel. Oliveira et al. [33] observed that these two stages are characterized by two distinct and subsequent peaks of contraction in the dilatometric curve. Speich et al. [34], Huang et al. [19], and Azizi-Alizamini et al. [23] concluded that austenite formation can be divided into two stages: (1) very rapid growth of austenite into pearlite until the complete dissolution of the pearlite and (2) slower growth of austenite into ferrite primarily controlled by carbon diffusion in austenite.

This divergence can be solved considering the nucleation mechanism because the growth of austenite is strongly affected by the nucleation sites and rate. The observed sites for nucleation of austenite growing in pearlite are the interfaces between ferrite and cementite platelets and the grain boundaries between pearlite colonies (especially triple junction points) [31]. The second site is the most advantageous from the point of view of surface energy considering the high angle boundary between pearlite-pearlite grain, while a single pearlite colony offers a larger amount of internal interfacial area but a lower mismatch between the ferrite-carbide lamellae [20]. On the other hand, nucleation can also take place at the pearlite-ferrite boundary for ferrite/pearlite steels [31]. Austenite has been also observed to form at the ferrite-ferrite grain boundaries. This was explained by the presence of cementite particles [19] and, more rarely, by the presence of retained austenite in the starting microstructure [29] and, for heating rate not very high, by the decreasing equilibrium of C content of ferrite at the increase of temperature [27].

In general, the austenite nucleation is then associated with cementite precipitates, the most favorable nucleation sites being the ferrite/pearlite interfaces followed by the pearlite/pearlite interfaces and, eventually, by the ferrite/ferrite interfaces. In any case, however, the measured advance rates of the austenite/pearlite front are much faster than those of the austenite/ferrite front; to this regard, much valuable data about austenite growth rate were measured by Schmidt et al. (2006) using an in situ visualization of the phase transformation by means of a confocal scanning laser microscope.

Short-range carbon diffusion between adjacent pearlitic cementite lamellae controls the austenite growth from prior pearlite. However, the diffusion of substitutional elements can also play a key role; for example, the growth of austenite during pearlite dissolution is much slower in presence of substitutional elements, as Mn (see below). On the contrary, the growing of austenite nucleated at ferrite/ferrite boundaries requires the carbon diffusion over relatively large distances from pearlite-nucleated austenite along with the parallel cumbersome diffusion of substitutional alloying elements. Thus, the

growth of austenite nucleated at pearlite sites and at the ferrite grain boundaries is in competition [19, 35]. Huang et al. [19] stated that the competition between austenite formed at these different sites is responsible for the marked heating rate effect on the austenitization kinetics.

Slow heating rates will favor the austenitization of the prior pearlite sites (see Fig. 5). In this case, the transformation of the pearlite will be completed before the one of the proeutectoid ferrite, which will be hampered because of limited carbon supply due to the few and isolates nucleation sites at the ferrite grain boundaries. The consequence is that the austenite will inherit the distribution of prior pearlite colonies.

High heating rates shift the transformation to higher temperatures and increase the superheating therefore promoting additional nucleation at the ferrite grain boundaries (see Fig. 6). The result is an increase in the nucleation site density with a consequent decrease of the average austenite grains size (see Fig. 6). In this scenario, the austenitization of pearlite and that of proeutectoid ferrite overlap.

After the transformation of the pearlitic ferrite, in accordance with the austenitization path undertaken, the structure can consist or of a mixture of austenite with untransformed proeutectoid ferrite at low heating rate (Fig. 5) or of austenite with partially dissolved pearlitic cementite and partially transformed proeutectoid ferrite at high heating rate (Fig. 6). As the austenitization proceeds further, the proeutectoid ferrite continues to transform; simultaneously, the thickness of the carbide lamellae, possibly retained, progressively reduces due to the additional amount of carbide dissolution occurred in the pearlite colonies.

It has to be pointed out that the dissolution of lamellar pearlite occurring during the first stage of austenitization in ferrite/pearlite steels generates a carbon-rich austenite, which is not in equilibrium with ferrite, as described by Katsamas [26], Clarke et al. [24], Gaude-Fugarolas [36], and Savran [20]. As a consequence, when the temperature rises above Ac_1, there are two carbon transfer mechanisms acting in the microstructure. The first one is the short-range diffusion in the pearlitic-generated austenite involving undissolved cementite lamellae and the second one is a long-range diffusion between pearlitic-generated austenite and the ferritic-generated austenite, the latter having a low carbon content.

The same process, but much more limited due to the lower diffusion coefficient, involves substitutional alloy elements, e.g., Mn and Cr, which has to diffuse in the forming austenite. To this regards, some authors talk of the rapid diffusion of carbon and the slow diffusion of the alloying elements at the ferrite/austenite interface [37]. Indeed, the presence of substitutional elements drastically influences the kinetics of austenitization for multicomponent steels [38]. For example, Atkinson et al. [39] showed that the addition of Si slows the transformation into austenite, while the addition of Mn
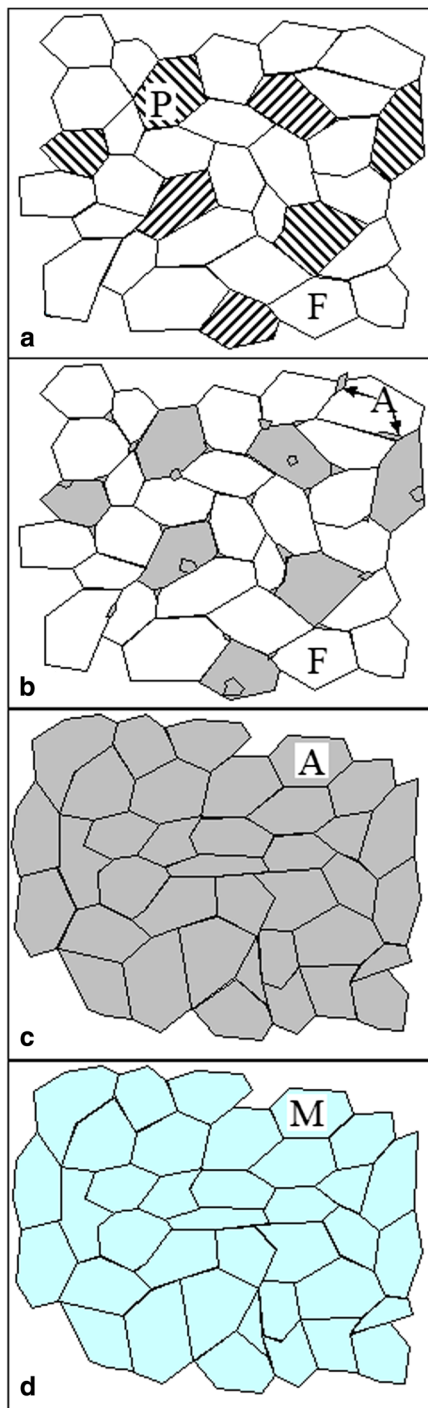
Fig. 5 Microstructure evolution during induction surface hardening of a ferrite/pearlite steel. **a** Initial microstructure. **b** Transformation of pearlite to austenite with low density of nucleation sites within the proeutectoid ferrite (low heating rate). **c** Transformation of proeutectoid ferrite to austenite. **d** Final quenching to obtain martensite
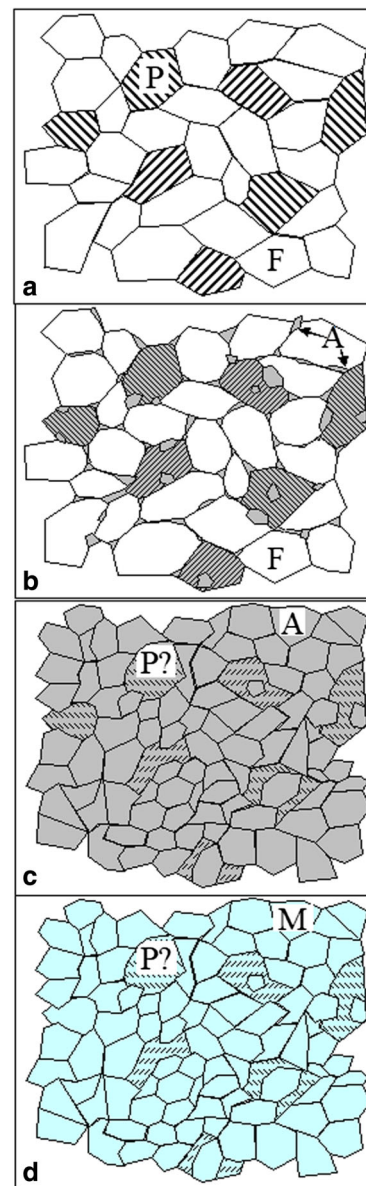
Fig. 6 Microstructure evolution during induction surface hardening of a ferrite/pearlite steel. **a** Initial microstructure. **b** Transformation of pearlitic ferrite to austenite and partial dissolution of lamellar cementite; high density of nucleation site within the proeutectoid ferrite (high heating rate). **c** Transformation of proeutectoid ferrite to austenite and further dissolution of lamellar cementite. **d** Final quenching to obtain martensite and probable pearlite ghosts

increases it, being the former a stabilizer of ferrite and the latter of austenite.

The austenitization of pearlite is then problematic for steel containing high amounts of alloying elements as Cr, Mo, or V.

They dissolve preferably within stable carbides increasing their stability, diffuse slowly, and slow down the diffusion of carbon. Furthermore, the solubility and diffusivity of carbon or other alloying elements are decreased by the presence of alloying elements like Cr, which delay the austenitization. On the other side, elements like Cr or Mo form stable carbides which limit the austenite growth [40, 41].

Then, the forming austenite is progressively enriched with carbon and is enriched or depleted of alloying elements according to the allowable equilibrium level and diffusion kinetics.

If the austenitization process is not given enough time, the dissolution of pearlitic cementite or proeutectoid ferrite may not be completed during the heating stage. This results in the preservation of some phases from the initial microstructure after the quenching, i.e., pearlitic cementite, or in general carbides, and ferrite [14]. For example, retained ferrite is visible inside the structure as big blocky white areas of undissolved ferrite [30].

Analogously, and this is valid especially for the pearlitic cementite, if the diffusion does not is have time to homogenize the structure after the cementite or ferrite dissolution, concentration gradients of carbon and alloying elements can remain in the resulting austenite. The transformed microstructure in which gradients in composition still persist is called inhomogeneous austenite. For example, concentration gradients, remnants of pearlite dissolution, called "pearlite ghosts," can often be observed after etching steel containing Cr. Concentration gradients of Mn or other alloying elements that do not alter the etching response like Cr cannot be visualized using optical or electrical micrographs [24]. Similarly, the scientific literature provides data of the austenite carbon content as a function of the austenitizing time for prior spheroidized ferrite/pearlite microstructure [14].

This phenomenon is very important since the microstructure and composition gradients developed during the heating stage are frozen by the subsequent quenching. The steel transforms in function of the local composition upon cooling so that the resulting microstructure will be a consequence of it. For example, Lee et al. [42] observed a decrease of Ms temperature of an AISI 52100 steel with the increase of the maximum temperature attained during the heating stage. This decrease was attributed to the increase of the carbon concentration in the transformed austenite due to the greater dissolution of cementite achieved at higher temperatures; it is remembered that Ms decreases with the increase of the carbon concentration in the austenite. The authors concluded that the Ms reduction correlates with the carbon concentration in the austenite because of its greater effect on Ms than other substitutional alloying elements. Measured values of Ms can be used to infer the carbon concentration in transformed austenite from a microstructure consisting of spheroidized carbides in a ferrite matrix by using Andrews' linear Ms equation [42]. In

addition, an uneven distribution of carbon in the austenite results in a low hardness of the resultant martensite, considering that the martensite hardness is mainly a function of its carbon content. To this regard, Clarke et al. [24] observed that the martensite obtained from induction hardening of hypoeutectoid steels attains maximum hardness, for the same treatment time, only when it is heated at temperatures above Ac_3 because the prior austenite structure does not reach homogenously distributed carbon concentration until higher temperatures are attained. Similar results can be obtained with a longer duration of the heating stage.

Similarly, concentration gradients of alloying elements other than carbon can be important for their final effect on the case microstructure. For example, segregation of alloying elements in zones of prior pearlitic cementite was observed by Clarke et al. [24], particularly of Cr and Mn. They concluded that longer heat treatments may be necessary to eliminate segregation, because after the austenite formation from the prior ferrite, the retained carbide dissolution is controlled not by carbon diffusion but by the much slower substitutional diffusion at interfaces. Similarly, Ågren [37] showed that the Mn enrichment in the austenite is of great importance because it stabilizes the austenite relative to the ferrite and thus increases the austenite hardenability. In the case of Mn segregation, the Mn-rich layers of austenite transform to martensite at lower temperatures and can be left untransformed after the quenching in case of high Mn content as well as for an increased carbon content caused by the strong affinity between C and Mn.

As expected, the scale of the initial microstructure strongly influences the austenitization kinetics. It has been reported that both the nucleation rate and the austenite growth rate increase with the decrease of the microstructure coarseness. Indeed, a decrease in the microstructure average dimension provides more potential nucleation sites and reduces the diffusion distances. There are many experimental data confirming that the nucleation and the growth rate of the austenite in a microstructure containing pearlite increase with the edge length of the pearlite colonies, i.e., inversely proportional to the area per unit volume of pearlite/pearlite colony interfaces, and decrease with the interlamellar spacing (see for example [14, 31, 43]).

Summarizing, the austenitization of a ferrite/pearlite steel at high heating rates can be described as follows:

1. High-rate transformation of the pearlitic ferrite to austenite and concomitant start of the dissolution of the pearlitic cementite into the austenite under formation at a slower rate
2. Growth of the austenite into the proeutectoid ferrite and dissolution of cementite retained form the previous stage; possible overlap between (2) and (1)

3. Completion of the transformation of the ferrite to austenite with resultant inhomogeneous structure
4. Homogenization of the austenite by means of the diffusion of carbon away from the original sites of the cementite lamellae. Other alloying elements also diffuse in this stage and flatten out their concentration gradients

The same sequence of events occurs during the austenitization of a fully pearlitic structure; the only difference is the absence of the austenitization of the proeutectoid ferrite. In this case, the pearlitic cementite is the last to austenitize.

3.2 Ferrite/carbide mixtures

Mixtures of ferrite and spheroidized cementite/carbides austenitize in two stages as observed experimentally by Miyamoto et al. [44], Chae et al. [45], and Lee et al. [46]. Firstly, the ferrite transforms to austenite with the contemporary start of the dissolution of the cementite (see Fig. 7). This process is driven by the carbon diffusion from the cementite to the forming austenite until the ferrite is totally consumed at the Ac_{f1}. At this stage, the carbon content of austenite rapidly increases, although the amount of austenite grows up, because the dissolution speed of the carbides is high (Molinder 1956). The rapid dissolution of cementite in the initial stage was proven by both experimental measurements and numerical calculations. Then, this dissolution gradually slows down due to the change of the concentration slope at the interface of both carbon and substitutional elements [47].

Austenite was observed to nucleate preferentially near intergranular carbides located on ferrite grain boundaries [45]. However, a limited amount of austenite nucleation was also observed at intragranular carbide as shown in Lai et al.. At the end of this stage, the structure is composed by austenite grains engulfing the remaining cementite particles (see Fig. 7). Afterwards, the residual cementite particles are dissolved into the austenite by carbon diffusion. At Ac_c, the cementite is consumed but the carbon distribution in the austenite is inhomogeneous, so that further time is needed until the carbon attains a homogeneous distribution into the austenite [48, 49].

Also in the case of ferrite/carbides particle microstructures, the presence of substitutional alloying elements affects the reverse transformation to austenite considering that they are inhomogeneously distributed; for example, it is known that in tempered martensite cementite/carbide are enriched in Mn while ferrite is enriched in Si or Al [42]. Such inhomogeneity makes the austenitization more difficult in alloyed steels both when the austenite growth is controlled by the carbon diffusion, the addition of these elements decreasing the carbon activity gradient, and when the diffusion of the alloying elements is necessary for austenite growth, as in the case of Cr-added steel. For example, Miyamoto et al. [44] reported that the reverse transformation kinetics from spheroidized ferrite/
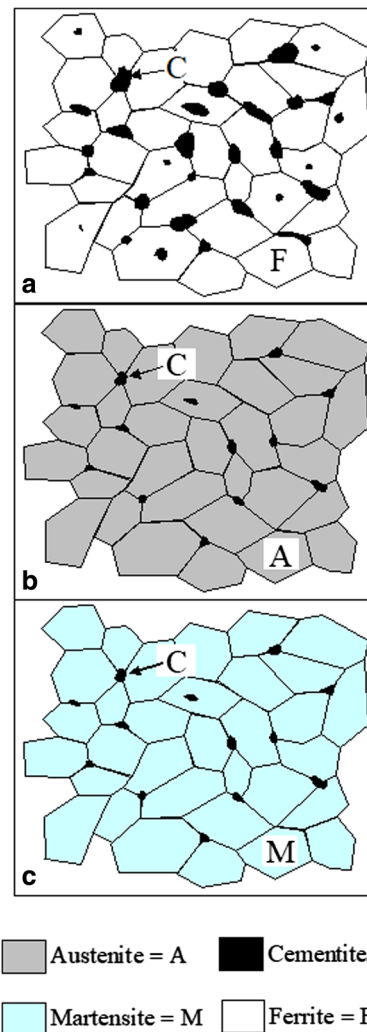
Fig. 7 Microstructure evolution during induction surface hardening of a ferrite/carbides aggregates steel. **a** Initial microstructure. **b** Transformation of ferrite to austenite and partial dissolution of cementite particles. **c** Final quenching to obtain martensite and probable remnants of carbides particle

cementite aggregates is slowed down by the addition of Mn, Si, and Cr. The retarding effect of Cr is particularly remarkable; indeed, it was found that the advance of the austenite/cementite interface is accompanied by Cr partitioning. Similarly, the analysis of Lai et al. [50] showed that for high Mn content in cementite, the austenite growth is essentially composed of a partitioning growth controlled by Mn diffusion in ferrite and a subsequent Mn diffusion in the austenite for the final equilibration. On the contrary, if the Mn content in the cementite is small, the initial negligible-partitioning growth controlled by carbon diffusion in austenite becomes significant and the transformation is so accelerated.

The inhomogeneous distribution of alloying elements can also influence the stability of the forming austenite. For example, Liu et al. [51] experimented that the Cr enrichment

observed during the dissolution of the carbide particles in a Fe-2.06Cr-3.91C steel brings about a supersaturated cementite which can decompose into austenite and Cr_7C_3. On the contrary, in case of Mn steel, the austenite/cementite interface advances without Mn partitioning and in doing so the forming austenite inherits the high Mn content of the cementite; that can cause the formation of retained austenite under quenching [44].

As in the case of ferrite/pearlite structure, the coarseness of the initial microstructure retards the austenitization kinetics; for example, it was observed that steels containing larger initial cementite particles exhibit slower reversion kinetics [44].

4 Heating rate effects

The response of steels to austenitization during induction surface hardening is very sensitive to the heating rate. Increasing the heating rate, indeed, increases the delay of the transformation, an effect known as the thermal hysteresis of steel [24]. This results in an increase of the start and finish transformation temperatures, both of the temperatures at which austenite formation starts and ends, and of the temperature at which the cementite or carbide dissolution is completed. The temperature of attainment of the thorough austenite homogenization is also affected by thermal hysteresis. Furthermore, it was demonstrated that the rise of the critical temperatures with heating rate depends on the initial microstructure of the steel, namely the coarser the initial structure is, the stronger is the thermal hysteresis effect, with a higher increase of the transformation temperatures. This dependence on the structure is influenced by the heating rate because the higher the heating rate is, the stronger the structure influence on the critical temperatures is. However, increasing the heating rate has a greater effect on Ac_3 than on Ac_1, which generally results less responsive to the variation of heating rate [24, 52]; so that as the heating rate increases $(Ac_3 - Ac_1)$ increase.

To this regard, valuable data about ferritic, ferritic/pearlitic, and pearlitic steels can be found in Clarke [14], Clarke et al. [24], and Caballero et al. [52]. Similar data about prior spheroidized cementite particles embedded in a ferrite matrix can be found in Mohanty et al. [53], Miyamoto et al. [44], and Clarke [14].

For example, Clarke et al. [24] demonstrated that, for an AISI 5150 steel, on-heating transformation temperatures are significantly higher for a hot rolled condition, with a ferrite/pearlite initial microstructure, than for a finer quenched and tempered prior microstructure. Furthermore, increasing the heating rate has a greater effect on transformation temperatures for the hot rolled initial microstructure than for the quenched and tempered prior condition. Likewise, Caballero et al. [52] and Caballero et al. [54] reported that for pearlitic steels, the larger the interlamellar spacing and area per unit

volume of the pearlite colonies interface are, the more they increase their critical temperature with the heating rate (see Fig. 8).

All the factors which retard the austenitization kinetics obviously increase the critical temperatures of the transformation, as already pointed out before. For example, the presence of some alloying elements, as Si which was demonstrated by Hernández-Morales et al. [55] to increase both the critical temperatures and the transformation temperature range.

It is important at this point to discuss the austenitization of cold worked steels since it is strongly affected by the heating rate. As a general rule, austenitization kinetics is accelerated by prior cold work [19, 23]. Cold working produces a deformed structure with grains elongated along the direction of the plastic flow and showing an aspect ratio consistent with
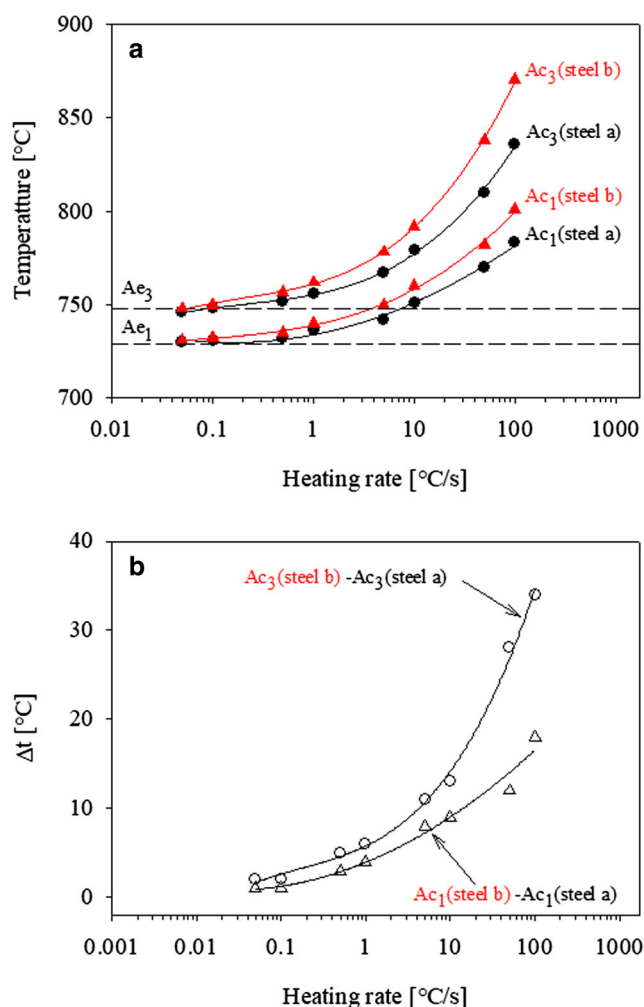
Fig. 8 Effect of heating rate and microstructure on Ac_1 and Ac_3 of two 0.76C-0.91Mn wt. pct. steels with a pure pearlitic initial microstructure. **a** Ac_1 and Ac_3 vs. heating rate. **b** Temperature differences (steel b − steel a) between Ac_1 and Ac_3 for each tested heating rate (steel a: average interlamellar spacing = 0.06 μm, area per unit volume of the pearlite colonies interface = 1432 mm^{-1}; steel b: average interlamellar spacing = 0.2 μm; area per unit volume of the pearlite colonies interface = 581 mm^{-1}). Data from Caballero et al. [52]

the level and direction of cold deformation. For example, cold rolling of pearlitic/ferritic steel produces a structure with both the ferrite grains and pearlite colonies aligned along the rolling direction. An increase of the dislocation density and then of the stored energy which supplies the driving force for recrystallization upon heating, an increase of the grain boundary area, and the breakup of the laminar structure of the pearlite are the final effect of cold working.

Whereas for non-deformed structure austenitization is the main process, for prior cold worked structures, recrystallization of deformed ferrite, spheroidization of broken cementite lamellae and austenite formation can occur and interact depending on the heating rate. The nucleation events are still crucial in this case as for the austenite formation in undeformed structures. As before, slower heating rates support the growth of austenite nucleated at prior pearlite areas, while higher heating rates stimulate additional nucleation at ferrite grain boundaries. However, nucleation at ferrite/ferrite grain boundaries can take place only at recrystallized grains, since moving ferrite grain boundaries under recrystallization do not provide suitable nucleation sites for austenite [19, 35]. Furthermore, the degree of spheroidization of carbide lamellae and of recrystallization of deformed ferrite grains is reduced with increasing the heating rate. Thus, the overlap between recrystallization and austenitization will encourage the growth of austenite grains from the prior pearlite colonies.

Under heating rates typical of induction hardening for normal steels, the recrystallization of deformed ferrite has generally concluded or has reached a great degree before sample reached the intercritical temperature range. In this case, the austenitization proceeds as for undeformed structures and a fine equiaxed structure can be obtained after austenitization, the only difference being dictated by the degree of spheroidization reached by the pearlite colonies (usually the spheroidization degree is low in induction heating). For low spheroidization, the austenite morphology engulfs the shape of the initial pearlite colonies which are basically elongated along the direction of the plastic flow, e.g., along the direction of cold rolling. Figure 9a–c schematizes the microstructure evolution according to this mechanism. The observed sequence is recrystallization, transformation of pearlitic ferrite to austenite and partial dissolution of pearlitic cementite particles, formation of nucleation sites within the proeutectoid ferrite, and final austenitization.

Increasing the heating rate, ferrite recrystallization and austenite formation can overlap more and more progressively. Partially recrystallized structures thwart the nucleation of austenite at nonstationary ferrite grain boundaries, thus encouraging the growth of austenite nucleated on deformed pearlite colonies (spheroidization of deformed cementite lamellae is hampered by high heating rate). Then, the growth occurs by means of lengthening and thickening of the former pearlite colonies rather than

additional nucleation on recrystallizing ferrite grain boundaries. The result is a banded structure of austenite characterized by block-like distribution that inherited the form of the prior pearlite colonies aligned along the flow direction. As it is imaginable, a more intense interaction between recrystallization and transformation leads to a more refined microstructure of the austenite. Figure 9a, d, e schematizes the microstructure evolution according to this mechanism. The observed sequence is transformation of pearlitic ferrite to austenite and partial dissolution of pearlitic cementite particles, overlap between growth of the austenite coming from pearlite and recrystallization of the cold worked ferrite (in this phase the lamellae of pearlitic cementite are further thinned), and complete austenitization with possible formation of pearlite ghosts.

Usually, a significant overlap of recrystallization and austenitization can be observed at the upper boundary of the heating rates typical of induction hardening, namely of the order of several thousand of kelvin per second. However, situations that obstruct the recrystallization can significantly decrease the heating rate needed to visualize this overlap, for example the presence of microalloying elements, as Ti and Nb, or of second phases with their pinning effect on grain growth. For example, Huang et al. [19] observed that approximately 90% of ferrite grains remained unrecrystallized at 100 K/s at the beginning of austenite formation in a 0.178C-1.55Mn-0.155Mo TRIP steel due to the presence of the Mo, which strongly delays recrystallization. Similarly, the opposite effect can be obtained adding Si that increases Ac_1 and then favors the ferrite recrystallization.

The heating rate effects can be easily visualized using continuous heating transformation (CHT) diagrams which are the analogous of the continuous cooling transformation diagrams. CHT diagrams are used to describe anisothermal on-heating transformations, especially for steels, and are an important tool to design and optimize thermal treatments such as induction hardening or intercritical annealing. Many studies have been performed to experimentally evaluate CHT diagrams for a wide range of steels characterized by various compositions, microstructures, and heating rates. The most important studies to this regard were proposed by Orlich et al. [56, 57], but very useful discussions about CHT can be also found in Clarke [14] and Lee et al. [42]. For example, Fig. 10 reports the comparison between the CHT diagrams of two AISI 52100 steels both with a microstructure of spheroidized carbides in a ferrite matrix, but one is characterized by an average carbide size of 0.44 μm and the other by an average carbide size of 0.70 μm. Data about Ac_1 and Ac_{f1} are experimental, while data about the carbide dissolution completion temperature, Ac_c, and austenite homogenization temperature were simulated. It is quite evident that while Ac_1 and

Fig. 9 Microstructure evolution during the austenitization of a cold worked ferritic/pearlitic steel. **a** Initial microstructure. **b, c** Sequence of events observed for normal heating rates. **d, e** Sequence of events observed for very high heating rates
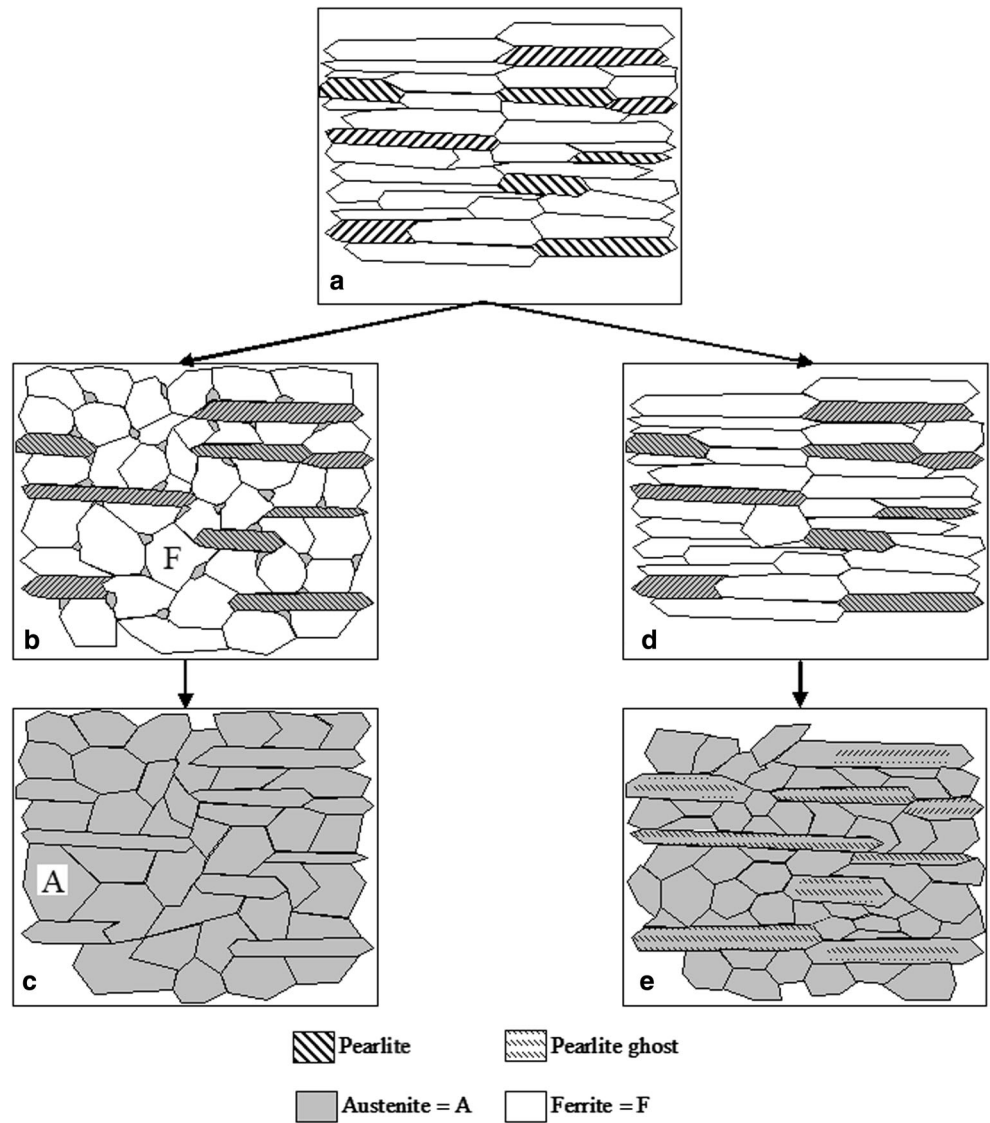
Fig. 10 CHT diagrams for two
spheroidized AISI 52100 steels
characterized by **a** a fine (average
carbide size = 0.44 μm, carbide
volume fraction 0.24) and **b**
coarse (average carbide size =
0.70 μm, carbide volume fraction
0.238) microstructure. Data from
Clarke [14]

Ⓢ Springer
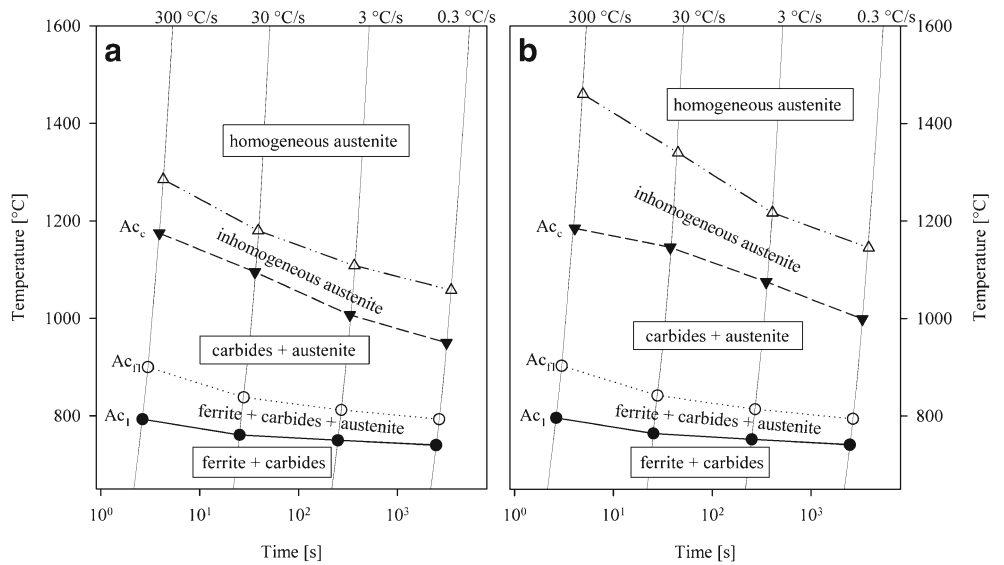
Ac_{fl} are slightly higher for the coarser morphology, yet the kinetics of the carbide dissolution and austenite homogenization are quite retarded increasing the carbide average dimension.

5 Austenite microstructure

The final austenite microstructure is the result of the competition among nucleation, growth, and grain coarsening. As already partially anticipated, many nuclei appear at high heating rate so that the nucleation dominates over the growth and the final grain size is smaller. On the contrary, longer heating times result in a larger grain growth that generates a coarse martensite and an extended transition zone. It was observed that fine-grained austenites are obtained with increasing the heating rate, with decreasing the holding time, and with increasing the amount of prior cold work [40, 58]. Some of these effects are synthesized in Fig. 11 which reports the prior austenite grain size as a function of the heating rate for a 50CrMo4 steel induction hardened at three different annealing temperatures (cooling rate of 280 K/s). The grain size decreases with the increase of the heating time and the decrease of the annealing temperature. Lesch et al. [60] observed that the alloying elements also play an important role in determining the prior austenite grain size. With an increasing amount of microalloying elements, the achievable mean grain sizes decrease significantly. Under the same cold work and annealing conditions for example, the grain size can be reduced by about two ASTM classes by microalloying with Ti or Nb.

According to the previous discussion, annealing temperatures just above Ac_3 in association with very short holding times should be applied to obtain a refined structure. Since these conditions are usually fulfilled during a well-designed induction surface hardening, a very refined microstructure with respect to the initial structure is normally achieved. This, along with a further grain refinement achieved after the quenching (see below), generates the well-known super-hardening phenomenon. Due to this phenomenon, the surface hardness of an induction-hardened steel can be 2–4 HRC higher than after a through-hardening treatment [61].

Typical prior austenite mean grain sizes obtainable by induction surface hardening range from ASTM G 12 to 8; for example, Vieweg et al. [59] observed a mean prior grain size of 12 μm for a ferritic/pearlitic 50CrMo4 steel (austenitized at 950 °C at 100 K/s), Hayashi et al. (2010) measured a value of 6 μm for a quenched and tempered 0.4Mo steel (austenitized at 1050 °C at 350 K/s, 1 s soaking time), and Yang et al. [18] a value of 21 μm for a quenched and tempered SAE 1070 steel (austenitized at 1036 °C at 250 K/s, 0.5 s soaking time).

The best results in terms of prior austenite grain size have been obtained through the double induction hardening
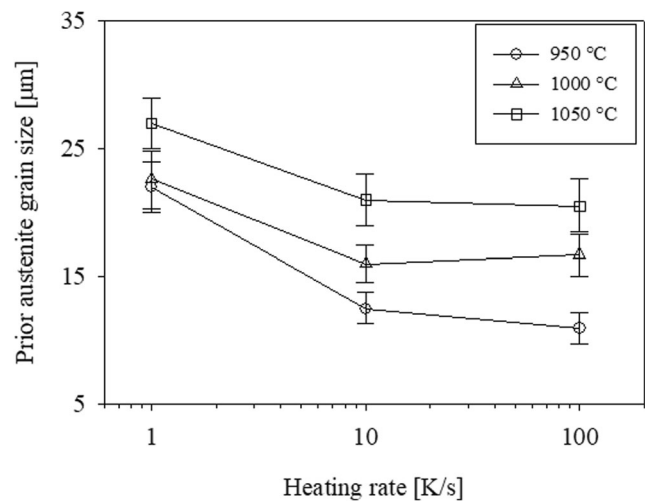
Fig. 11 Effect of heating rate and maximum heating temperature, 950, 1000, and 1050 °C, on prior austenite grain size for 50CrMo4 steel. Redrawn from Vieweg et al. [59]

treatment which performs a rapid heating and rapid cooling of the part twice [62]. The double treatment can be varied in many ways, e.g., a higher annealing temperature can be used for the first stage followed by a second treatment at lower temperature. Generally, the aim of the first treatment is to produce a satisfactorily homogeneous carbon distribution, whereas the desired hardened layer is obtained through the second treatment. This process produces a remarkable refinement of the prior austenite grain, especially in presence of inhibitors of the grain growth [58, 63]. To this regard, Hayashi et al. [58] claim to have invented a new steel containing 0.4% by weight of Mo which subjected to the double induction hardening (heating to 1050 °C at 350 K/s and quenching, followed by a re-heating to 950 °C at 350 K/s and quenching) develops a prior austenite grain size as small as 3 μm.

As already pointed out, the material undergoes different thermal cycles as function of the distance below the surface, experiencing then differential treatments from the surface toward the workpiece core. Hence, the austenitization dynamics generate a profile of prior austenite microstructure from the surface toward the workpiece core at the end of the austenitization process. In particular, three zones can be distinguished at this stage: the fully austenitized zone, close to the surface (henceforth called austenitic zone), the zone farthest away from the surface, unaffected by the heat treatment (subsequently called unaffected zone), and the zone intermediate between the previous ones (afterwards called intermediate zone) (see Fig. 12). After the quenching, this zone along with the part of the austenitic zone which possibly is not cooled fast enough to reach the required hardness constitutes the transition zone of the hardened case [13, 64, 65]. The transition zone is the part of the total case that may include a
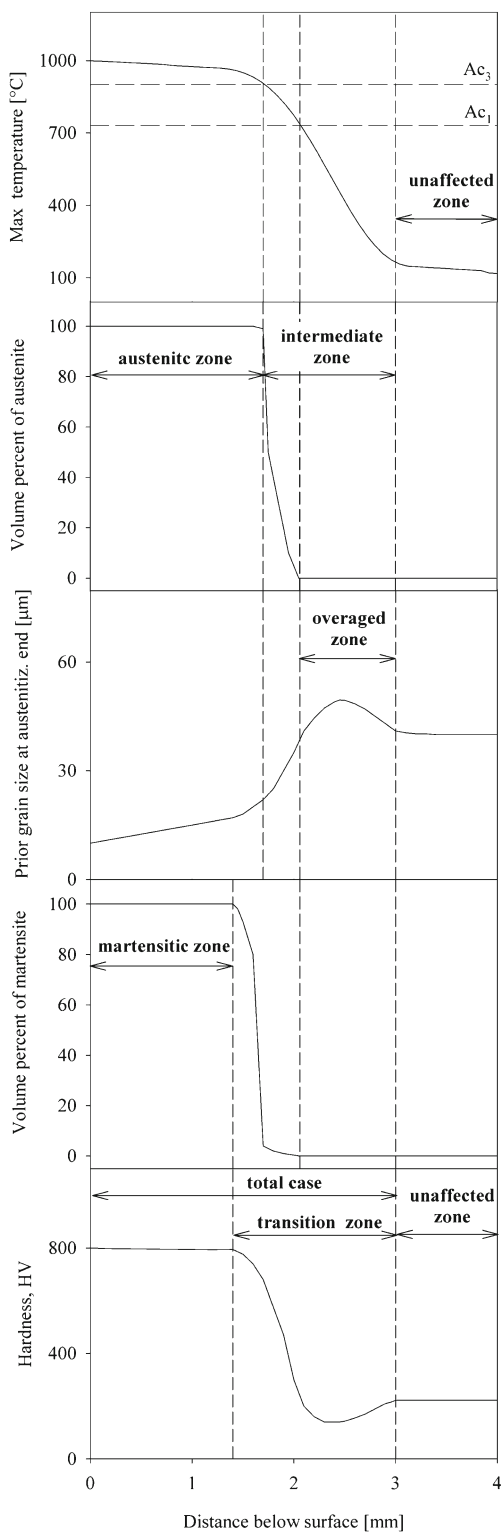
Fig. 12 Qualitative description of the typical distribution of peak temperature, austenite and martensite content, prior grain size at the end of the austenitization, and hardness along the workpiece thickness
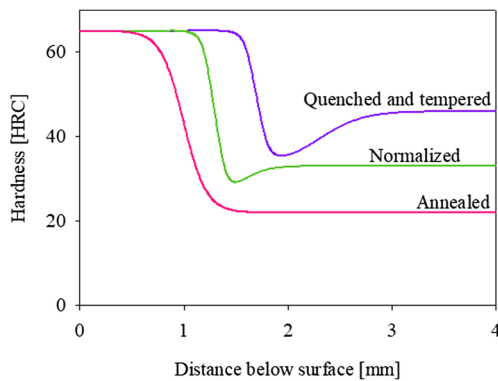
coincides with the austenitic one in typical induction surface hardening practise, so that usually the transition zone is the resultant of the intermediate zone. On its own, the intermediate zone can be subdivided in two parts going deeper into the workpiece from the surface (see Fig. 12). The first part is the one that was annealed within the intercritical region so that its microstructure is only partially composed by austenite. The second part did not experience any austenitization process, since it did not reach Ac_1. Nonetheless, its structure is different from that of the unaffected zone having been subjected to temperature rise that can have activated recovery processes, grain growth, and recrystallization, as it will be explained below.

The workpiece experiences different thermal cycles along its thickness; the heating rate and the maximum annealing temperature normally decrease going from the surface to the core. Then, according to what was previously exposed, two phenomena are operative. Firstly, going toward the workpiece core, the growth of austenite is favored over its nucleation; this promotes a coarsening of the obtained austenite grains. On the other hand, starting from the depth at which the maximum temperature reached is Ac_3, overaging of the untransformed volume fraction is active, especially where temperatures exceed 500–600 °C. This induces grain coarsening, recrystallization, and recovery (especially for cold worked materials) and brings about a softening of the material. The importance of softening is higher the higher the attained temperature is and the lower the volume fraction of the austenite is. In particular, softening can be quite important in the region of the treated layer which is heated below Ac_1, considering that there are no phase transformation there.

Accordingly, a gradient of prior austenite grain size develops along the thickness (see Fig. 12). This is characterized by an increase of the grain size from the surface to the unaffected material. It is to be noted that the prior grain size of the intermediate region which was heated below Ac_1 is larger than that of the unaffected zone, since it was subjected only to overaging and not to austenitization. When the temperature of the subsurface exceeds the temperature of the surface or its dwell at high temperatures exceeds that of the surface, then another maximum in grain size is observed in the subsurface, as demonstrated by Yang et al. (2010).

Figure 12 tries to rationalize the previous discussion showing the qualitative extent of the abovementioned zones with the distribution along the workpiece thickness of the maximum reached temperatures. To be noted, the hardness decay is displayed by the overaged zone.

It is quite obvious at this point that the initial microstructure has a pronounced effect on the shape and extension of the previous zones, especially on the transition one. Figure 13 reports the hardness profiles obtained applying the same induction hardening process to three steels of same composition but different initial microstructure. Finer structures, as the

combination of martensite, bainite, pearlite, and ferrite, while the most superficial part of the case is predominantly martensitic. It has to be said, however, that the martensitic zone

Fig. 13 Hardness profiles obtained in three AISI 1060 steel bars in dependence of the initial microstructures (induction generator operating at 400 kHz with a power density of 2.5 kW/cm^2)

quenched and tempered, are more favorable to austenitization, according to the previous discussion: this produces a deeper effective case compared with other structures. However, fine microstructures are also keener on undergoing softening processes into the overaged zone. Hence, for this structure, the larger transition zone is observed, with the larger hardness decay as regards the unaffected material. The initial annealed structure in Fig. 13 develops the smaller austenitic zone, power density, and treatment time being equal, so that it results in the shorter effective case. Softening effects are absent in the transition zone of the annealed structures considering that annealing produces equilibrium microstructures.

6 Microstructure of the hardened case

The quenching, the final stage of the process, acts on such a complex parent microstructure. The features that most influence the lath martensitic structure and hardness of the case are the non-homogenous concentration of carbon and substitutional alloying elements and the dimension of the parent austenite structure.

The lath martensite structure is hierarchical. Indeed, any prior austenite grain is divided into several packets, which are subdivided into blocks. Each block contains a group of laths with almost the same orientation. Blocks which accommodate laths with almost the same habit plane are grouped into the same pocket. Since packets and blocks form high angle boundaries, they are like affective grains and act as barriers for the dislocation motion during plastic deformation [66]. It is known that the strength and toughness of lath martensite structures are improved with the decrease in packet and block size [67, 68]. The packet dimension and block size of the martensite decrease with increasing the carbon content, as demonstrated by [69, 70]. The packets, blocks, and laths are also refined by increasing the cooling rate [71, 72].

On the other hand, both the block width and the packet size are proportional to the prior austenite grain size, so that the prior austenite grain size plays a role in controlling the strength and toughness of the lath martensitic structure [67, 73]. To this aim, the refinement of the prior austenite grains can be used to induce the refinement of the martensitic packets and blocks [74].

The carbon content of the parent austenite is also to be taken into account. The hardness of the martensite and the amount of retained austenite markedly increase with the increase of the carbon content, as reported by Krauss [75]. Retained austenite bears the risk of dimensional instability and can spoil the finishing or hardness of the treated surface. Carbon content also influences the autotempering phenomena, because Ms decreases with increasing the carbon concentration [75, 76]; a high Ms leads to a potential autotempering of the martensite during the cooling after the martensitic transformation. Autotempering reduces the hardness of the martensite improving its ductility and should be usually avoided in induction surface hardening. Moreover, the decrease of Ms with the increase of the carbon content is the cause of the increase of the retained austenite with the carbon content, as demonstrated by Koistinen and Marburger [77] and Harris and Cohen [78]. Finally, the dislocation density in martensite is strongly related to the carbon content in solution [69, 79]. In particular, the dislocation density and thus the strength increase with the carbon of the martensite.

The homogenization of the carbon concentration during the heating phase is then critical to maximize the hardness of the resulting martensitic case. It was demonstrated that the hardness of the case increases with the maximum temperature attained during the austenitization; however, a plateau is eventually reached, so that the case hardness does not increase any further for any increase of the austenitization temperature above this point [14, 24]. This threshold value of the temperature increases with the heating rate. On the other hand, the maximum hardness is just a function of the carbon content and not of the initial microstructure (Fig. 14).

The final microstructure of the case is then constituted by lath martensite with block and packet size which normally increase from the surface toward the material core or at least follow the size gradient of the parent austenite grains (see Fig. 12). Due to the presence of carbon inhomogeneity, the effective case can show retained austenite, which was observed by Clarke [14] for example, and non-martensitic products, as bainite or acicular ferrite and even pearlite [24, 40]. Tempered martensite and fine precipitated carbides in zones of low carbon content can also be present due to some degree of autotempering.

Residual stresses associated with the hardened case are another critical factor in induction surface hardening. The martensite formation, with the associated expansion that takes place during the transformation, results in a substantial surface

Fig. 14 Hardness vs. maximum annealing temperature at different heating rate (HR) for induction hardened ASTM A322-07 steel with two initial microstructures. **a** Hot rolled. **b** Quenched and tempered. Redrawn after Clarke et al. [24]
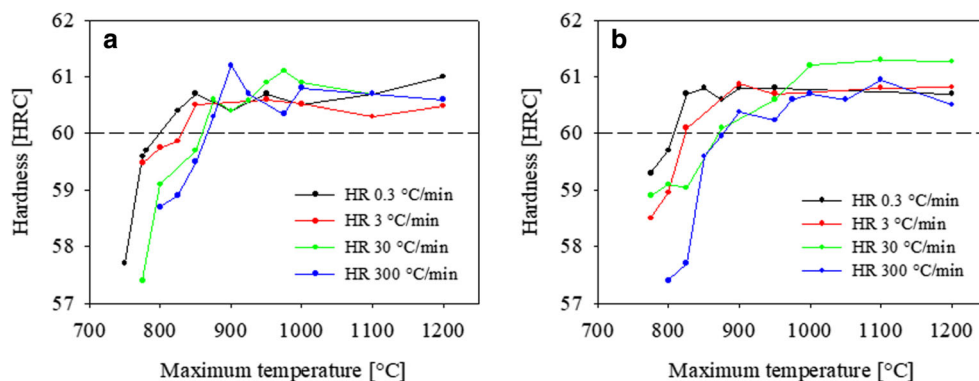
compressive residual stress in a majority of induction surface hardening applications [13, 80–82]. For the most employed shapes, i.e., planar or cylindrical, which represent the majority of the practical cases, the directions of the principal compressive stresses run parallel to the surface, while the other principal stress, normal to the surface, is almost zero, so that a plane residual stress state can be assumed [83]. Complicate situations can happen considering that the final residual stress state of a component arises from the overlap of residual stresses produced by the different phases of its manufacturing process.

Considering that profiles of microstructure and hardness are present into the total case and that they influence the material response to the strain caused by the expansion due to the displasive transformation, a residual stress profile is generated by induction hardening. The peak of the compressive stress is registered at the surface Fig. 15, but it can also be observed in the subsurface in the special case in which the maximum martensite content is developed at the subsurface, as previously discussed [84]. The high compressive residual stress state needs to be balanced by a tensile stress. The transition from compression to tensile stress marks the end of the hardened case. More precisely, the residual tensile stress develops into the softer zones adjacent to the effective case, namely into the transition zone and partially into the unaffected material. This generates a residual tensile stress peak in the transition zone. The profile of the tensile residual stress and of the compressive/tensile transition depends on the shape and width of the transition zone. Smooth transition zones generate a smooth compressive/tensile transition of the residual stress which in this case is characterized by a broad tensile peak and a slow decrease toward the workpiece core. On the contrary, narrow transition zones produce a more pronounced peak of the residual tensile stress with a steeper drop toward the core. Obviously, a higher residual tensile peak corresponds to a higher hardness in the transition zone. For example, Fig. 15

reports the qualitative profile of the residual circumferential stress which arises in a steel cylinder subjected to induction surface hardening as function of the initial microstructure. Due to the higher hardness and smoothness of its hardness profile across the transition zone, the quenched and tempered initial microstructure reaches a higher tensile peak than the starting normalized structure; moreover, the quenched and tempered microstructure presents a smoother compression/tension transition at the deep end of the case.

While the residual compressive stress of the hardened case acts as a crack arrester and increases torsional and bending fatigue life, the tensile peak of the transition zone can cause serious risk of fatigue failure, especially when it is associated with pre-existing residual tensile state, as the ones generated by machining operations prior to the induction hardening. Decreasing the transition zone can be highly detrimental from this point of view, considering that a sharp transition zone can be associated with a higher residual tensile peck.
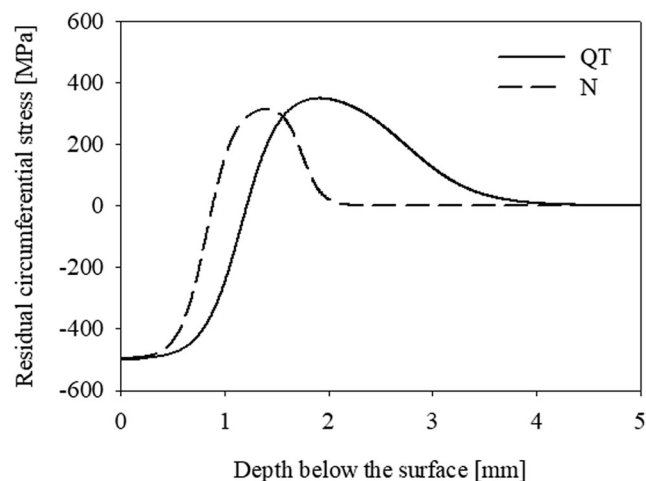
Fig. 15 Qualitative profile of the residual circumferential stress in a normalized (N) and quenched and tempered (QT) steel. Elaboration of data from Kristoffersen and Vomacka, Coupard et al., and Holmberg et al. [80, 82, 84]

7 Conclusions

The structure of the superficial layer of steels treated by induction surface hardening is very complex. Its main characteristics are as follows:

- A hardened case located close to the surface. This is a zone of high and constant hardness with a fully martensitic structure (Fig. 12).
- A transition zone between the hardened case and the unaffected material. It shows a decreasing profile of hardness with minimum values sometimes lower than that of the base material (Fig. 13). Its structure can include a combination of martensite, bainite, pearlite, and ferrite
- A profile of residual stresses with a marked compressive stress at the surface balanced by a tensional residual peak into the transition zone (Fig. 15).
- A size of prior austenite grains which increases from the surface to the base material and, due to overaging phenomena, can reach a maximum in the transition zone (Fig. 12).

The relative dimensions of the abovementioned zones and the shapes of the abovementioned profiles of hardness and grain size are strongly dependent on the applied thermal cycle, composition, and initial microstructure of the treated steel.

References

1. Gao K, Qin XP, Wang Z, Chen H, Zhu SX, Liu YX, Song YL (2014) Numerical and experimental analysis of 3D spot induction hardening of AISI 1045 steel. J Mater Process Technol 214(11):2425–2433. https://doi.org/10.1016/j.jmatprotec.2014.05.010

2. Shokouhmand H, Ghaffari S (2012) Thermal analysis of moving induction heating of a hollow cylinder with subsequent spray cooling: effect of velocity, initial position of coil, and geometry. Appl Math Model 36(9):4304–4323. https://doi.org/10.1016/j.apm.2011.11.058

3. Vieweg A, Ressel G, Prevedel P, Raninger P, Panzenböck M, Marsoner S, Ebner R (2016) Induction hardening: differences to a conventional heat treatment process and optimization of its parameters. IOP Conference Series: Materials Science and Engineering 119(1):012019

4. Kobayashi S, Takahashi H, Kamada Y (2013) Evaluation of case depth in induction-hardened steels: magnetic hysteresis measurements and hardness-depth profiling by differential permeability analysis. J Magn Magn Mater 343:112–118. https://doi.org/10.1016/j.jmmm.2013.04.082

5. Ceschini L, Martini C, Morri A (2015) Dry sliding wear of an induction-hardened, high-silicon medium-carbon microalloyed steel. Tribol Int 92:493–502. https://doi.org/10.1016/j.triboint.2015.07.032

6. Zhu SX, Wang Z, Qin XP, Mao HJ, Gao K (2016) Theoretical and experimental analysis of two-pass spot continual induction hardening of AISI 1045 steel. J Mater Process Technol 229:814–825. https://doi.org/10.1016/j.jmatprotec.2015.10.025

7. Gao K, Qin XP, Wang Z, Zhu SX (2016) Effect of spot continual induction hardening on the microstructure of steels: comparison between AISI 1045 and 5140 steels. Mat Sci Eng A 651:535–547. https://doi.org/10.1016/j.msea.2015.11.012

8. Lolla T, Cola G, Narayanan B, Alexandrov B, Babu SS (2011) Development of rapid heating and cooling (flash processing) process to produce advanced high strength steel microstructures. Mater Sci Technol 27(5):863–875. https://doi.org/10.1179/174328409x433813

9. Fett GA (2014) Induction case hardening of axle shafts. In: Rudnev V, Totten GE (eds) Induction heating and heat treatment, vol 4C. Vol ASM handbook. ASM International, pp 160–172

10. Li HP, He LF, Gai K, Jiang R, Zhang CZ, Li MS (2015) Numerical simulation and experimental investigation on the induction hardening of a ball screw. Mater Des 87:863–876. https://doi.org/10.1016/j.matdes.2015.08.094

11. Totik Y, Sadeler R, Altun H, Gavgali A (2003) The effects of induction hardening on wear properties of AISI 4140 steel in dry sliding conditions. Mater Des 24(1):25–30. https://doi.org/10.1016/S0261-3069(02)00099-7

12. Choi BY, Shin JH, Bahng GW, Yoon KB (1996) Metallographic study on rolling contact fatigue of 0.44%C-1.71%Mn induction-hardened bearing steels. Wear 192(1–2):1–5. https://doi.org/10.1016/0043-1648(95)06767-1

13. Rudnev V (2014) Principles of induction hardening and inspection. In: Rudnev VT, Totten G.E. (eds) Induction heating and heat treatment, ASM handbook Volume 4C. ASM International, pp 160–172

14. Clarke K (2008) The effect of heating rate and microstructural scale on austenite formation, austenite homogenization, and as-quenched microstructure in three induction hardenable steels. Ph.D. thesis, Colorado School of Mines, Golden, CO, USA

15. Ericsson T (1985) Thermal and austenitic thermochemical surface hardening of steel. In: Niku-Lari A (ed) Advances in surface treatments, vol 2. Pergamon Press, Oxford, pp 1–20

16. Rudnev V (2004) A common misassumption in induction hardening. Heat Treating Progress, vol SEPTEMBER/OCTOBER 2004

17. Brown D, Rudnev V, Dickson P (2014) Induction heating of billets, rods, and bars. In: Rudnev V, Totten GE (eds) Induction heating and heat treatment, ASM handbook Volume 4C. ASM International, Materials Park OH, pp 330–345

18. Yang BJ, Hattiangadi A, Li WZ, Zhou GF, McGreevy TE (2010) Simulation of steel microstructure evolution during induction heating. Mat Sci Eng A 527(12):2978–2984. https://doi.org/10.1016/j.msea.2010.01.038

19. Huang J, Poole WJ, Militzer M (2004) Austenite formation during intercritical annealing. Metall Mater Trans A 35a(11):3363–3375. https://doi.org/10.1007/s11661-004-0173-x

20. Savran VI (2009) Austenite formation in C-Mn steel. PhD thesis, Delft University of Technology,

21. Savran VI, Offerman SE, van Dijk NH, Lauridsen EM, Margulies L, Sietsma J (2007) Growth of individual austenite grains measured with 3DXRD microscopy. Pricm 6: Sixth Pacific Rim International

Conference on Advanced Materials and Processing, Pts 1–3 561-565:2301-+. doi:10.4028/www.scientific.net/MSF.561-565.2301

22. Speich GR, Demarest VA, Miller RL (1981) Formation of austenite during intercritical annealing of dual-phase steels. Metall Mater Trans A 12(8):1419–1428. https://doi.org/10.1007/BF02643686

23. Azizi-Alizamini H, Militzer M, Poole WJ (2011) Austenite formation in plain low-carbon steels. Metall Mater Trans A 42(6):1544–1557. https://doi.org/10.1007/s11661-010-0551-5

24. Clarke KD, Van Tyne CJ, Vigil CJ, Hackenberg RE (2011) Induction hardening 5150 steel: effects of initial microstructure and heating rate. J Mater Eng Perform 20(2):161–168. https://doi.org/10.1007/s11665-010-9825-8

25. Molinder G (1956) A quantitative study of the formation of austenite and the solution of cementite at different austenitizing temperatures for a 1.27% carbon steel. Acta Metall 4(6):565–571

26. Katsamas AI (2007) A computational study of austenite formation kinetics in rapidly heated steels. Surf Coat Tech 201(14):6414–6422. https://doi.org/10.1016/j.surfcoat.2006.12.014

27. Savran VI, Van Leeuwen Y, Hanlon DN, Kwakernaak C, Sloof WG, Sietsma J (2007) Microstructural features of austenite formation in C35 and C45 alloys. Metall Mater Trans A 38a(5):946–955. https://doi.org/10.1007/s11661-007-9128-3

28. Dykhuizen RC, Robino CV, Knorovsky GA (1999) A method for extracting phase change kinetics from dilatation for multistep transformations: austenitization of a low carbon steel. Metall Mater Trans B Process Metall Mater Process Sci 30(1):107–117. https://doi.org/10.1007/s11663-999-0011-z

29. Jayaswal SK, Gupta SP (1992) Kinetics of ferrite to austenite transformation in a high-strength low-alloy steel containing Ti and V. Z Metallk 83(11):809–819

30. Puskar JDD, R. C, Robino CV, Burnett ME, Kelley JB (1999) Austeriite formation kinetics during rapid heating in a microalloyed steel. DOE's Office of Scientific and Technical Information (OSTI)

31. Schmidt E, Wang Y, Sridhar S (2006) A study of nonisothermal austenite formation and decomposition in Fe-C-Mn alloys. Metall Mater Trans A 37a(6):1799–1810. https://doi.org/10.1007/s11661-006-0122-y

32. de Andres CG, Caballero FG, Capdevila C (1998) Dilatometric characterization of pearlite dissolution in 0.1C-0.5Mn low carbon low manganese steel. Scripta Mater 38(12):1835–1842. https://doi.org/10.1016/S1359-6462(98)00131-6

33. Oliveira FLG, Andrade MS, Cota AB (2007) Kinetics of austenite formation during continuous heating in a low carbon steel. Mater Charact 58(3):256–261. https://doi.org/10.1016/j.matchar.2006.04.027

34. Speich GRS,A, Speich GR, Richards MJ (1969) Formation of austenite from ferrite and ferrite-carbide aggregates. Trans Metall Soc AIME 245:1063–1074

35. Li P, Li J, Meng QG, Hu WB, Xu DC (2013) Effect of heating rate on ferrite recrystallization and austenite formation of cold-roll dual phase steel. J Alloys Compd 578:320–327. https://doi.org/10.1016/j.jallcom.2013.05.226

36. Gaude-Fugarolas D Phase transformations in steel during induction hardening. In: Makhnenko VI (ed) Mathematical modelling and information technologies in welding and related processes. Katsiveli, Crimea, Ukraine, 16–20 September 2002. International Association «Welding»,

37. Ågren J (1982) Computer simulations of the austenite/ferrite diffusional transformations in low alloyed steels. Acta Metall 30(4):841–851. https://doi.org/10.1016/0001-6160(82)90082-7

38. Ågren J, Vassilev GP (1984) Computer simulations of cementite dissolution in austenite. Mat Sci Eng 64(1):95–103. https://doi.org/10.1016/0025-5416(84)90076-4

39. Atkinson C, Akbay T, Reed RC (1995) Theory for reaustenitisation from ferrite/cementite mixtures in Fe-C-X steels. Acta Metall Mater 43(5):2013–2031. https://doi.org/10.1016/0956-7151(94)00366-P

40. Wendel M, Hoffmann F, Datchary W (2016) Bearing steels for induction hardening—part I. J Heat Treat Mat 71(1):20–34. https://doi.org/10.3139/105.110277

41. Wendel M, Hoffmann F, Datchary W (2016) Bearing steels for induction hardening—part II. J Heat Treat Mat 71(5):218–229. https://doi.org/10.3139/105.110299

42. Lee SJ, Clarke KD (2010) A conversional model for austenite formation in hypereutectoid steels. Metall Mater Trans A 41a(12):3027–3031. https://doi.org/10.1007/s11661-010-0418-9

43. Caballero FG, Capdevila C, de Andres CG (2000) Influence of scale parameters of pearlite on the kinetics of anisothermal pearlite-to-austenite transformation in a eutectoid steel. Scripta Mater 42(12):1159–1165. https://doi.org/10.1016/S1359-6462(00)00352-3

44. Miyamoto G, Usuki H, Li ZD, Furuhara T (2010) Effects of Mn, Si and Cr addition on reverse transformation at 1073 K from spheroidized cementite structure in Fe-0.6 mass% C alloy. Acta Mater 58(13):4492–4502. https://doi.org/10.1016/j.actamat.2010.04.045

45. Chae JY, Jang JH, Zhang G, Kim KH, Lee JS, Bhadeshia HKDH, Suh DW (2011) Dilatometric analysis of cementite dissolution in hypereutectoid steels containing Cr. Scripta Mater 65(3):245–248. https://doi.org/10.1016/j.scriptamat.2011.04.018

46. Lee SJ, Clarke KD (2015) A quantitative investigation of cementite dissolution kinetics for continuous heating of hypereutectoid steel. Metall Mater Trans A 46a(9):3917–3923. https://doi.org/10.1007/s11661-015-2995-0

47. Zhao L, Vermolen FJ, Wauthier A, Sietsma J (2006) Cementite dissolution at 860 degrees C in an Fe-Cr-C steel. Metall Mater Trans A 37a (6):1841–1850. doi:DOI https://doi.org/10.1007/s11661-006-0127-6, 37

48. Lee S-J, Clarke KD (2010) A conversional model for austenite formation in hypereutectoid steels. Metall Mater Trans A 41(12):3027–3031. https://doi.org/10.1007/s11661-010-0418-9

49. Lee S-J, Clarke KD (2015) A quantitative investigation of cementite dissolution kinetics for continuous heating of hypereutectoid steel. Metall Mater Trans A 46(9):3917–3923. https://doi.org/10.1007/s11661-015-2995-0

50. Lai Q, Goune M, Perlade A, Pardoen T, Jacques P, Bouaziz O, Brechet Y (2016) Mechanism of austenite formation from spheroidized microstructure in an intermediate Fe-0.1C-3.5Mn steel. Metall Mater Trans A 47a(7):3375–3386. https://doi.org/10.1007/s11661-016-3547-y

51. Liu ZK, Hoglund L, Jonsson B, Agren J (1991) An experimental and theoretical-study of cementite dissolution in an Fe-Cr-C alloy. Metall Trans A 22(8):1745–1752. https://doi.org/10.1007/Bf02646498

52. Caballero FG, Capdevila C, De Andres CG (2003) An attempt to establish the variables that most directly influence the austenite formation process in steels. ISIJ Int 43(5):726–735. https://doi.org/10.2355/isijinternational.43.726

53. Mohanty RR, Girina OA, Fonstein NM (2011) Effect of heating rate on the austenite formation in low-carbon high-strength steels annealed in the intercritical region. Metall Mater Trans A 42a(12):3680–3690. https://doi.org/10.1007/s11661-011-0753-5

54. Caballero FG, Capdevila C, De Andres CG (2001) Influence of pearlite morphology and heating rate on the kinetics of continuously heated austenite formation in a eutectoid steel. Metall Mater Trans A 32(6):1283–1291. https://doi.org/10.1007/s11661-001-0218-3

55. Hernández-Morales BV-G,O, López-Martínez E, Vergara-Hernández HJ, Olmos L (2014) Effect of heating rate and silicon content on kinetics of austenite formation during continuous heating. Mater Sci Forum 783-786:771–776

56. Orlich JP,H-J (1976) Zeit-Temperatur-Austenitisierung-Schaubilder. In: Atlas zur Wärmebehandlung der Stähle, vol 4. Verlag Stahleisen, Düsseldorf, Germany

57. Orlich JR,A, Wiest P (1973) Zeit-Temperatur-Austenitisierung-Schaubilder. In: Atlas zur Wärmebehandlung der Stähle, vol 3. Verlag Stahleisen, Düsseldorf, Germany

58. Hayashi TKN, Yamada K. (2010) Method of prior austenite grain refining using induction hardening. JFE Steel Corporation

59. Vieweg A, Ressel G, Prevedel P, Marsoner S, Ebner R (2017) Effects of the inductive hardening process on the martensitic structure of a 50CrMo4 steel. J Heat Treat Mat 72(1):3–9. https://doi.org/10.3139/105.110308

60. Lesch C, Alvarez P, Bleck W, Sevillano JG (2007) Rapid transformation annealing: a novel method for grain refinement of cold-rolled low-carbon steels. Metall Mater Trans A 38a(9):1882–1890. https://doi.org/10.1007/s11661-006-9052-y

61. Rudnev V (2008) Metallurgical insights for induction heat treaters—part 5: super-hardening phenomenon. Heat Treating Prog:35–37

62. Prabhudev KH (1989) Handbook of heat treatment of steels. McGraw-Hill, USA

63. Fujita E, Ogura Y, Kawasaki S, Kojima S, Makita S, Maeda S, Yamane H, Yoshida S (2014) Manufacturing method of high-strength and high-toughness thin steel and heat treatment apparatus. U.S. Patent,

64. Rudnev V (2005) Be aware of the 'fine print' in the science of metallurgy of induction hardening: part 1. Ind Heat March 2005: 37–42

65. Rudnev V (2005) Be aware of the 'fine print' in the science of metallurgy of induction hardening: part 2. Ind Heat May 2005: 41–47

66. Morito S, Yoshida H, Maki T, Huang X (2006) Effect of block size on the strength of lath martensite in low carbon steels. Mat Sci Eng A 438:237–240. https://doi.org/10.1016/j.msea.2005.12.048

67. Tomita Y, Okabayashi K (1986) Effect of microstructure on strength and toughness of heat-treated low-alloy structural-steels. Metall Trans A 17(7):1203–1209. https://doi.org/10.1007/Bf02665319

68. Swarr T, Krauss G (1976) The effect of structure on the deformation of as-quenched and tempered martensite in an Fe-0.2 pct C alloy. Metall Trans A 7(1):41–48. https://doi.org/10.1007/BF02644037

69. Sackl S, Leitner H, Zuber M, Clemens H, Primig S (2014) Induction hardening vs conventional hardening of a heat treatable steel. Metall Mater Trans A 45a(12):5657–5666. https://doi.org/10.1007/s11661-014-2518-4

70. Morito S, Tanaka H, Konishi R, Furuhara T, Maki T (2003) The morphology and crystallography of lath martensite in Fe-C alloys. Acta Mater 51(6):1789–1799. https://doi.org/10.1016/S1359-6454(02)00577-3

71. Morito SI,R, Kamiya K, Ohba T, Maki T (2010) Effect of cooling rate on morphology and crystallography of lath martensite in Fe-Ni alloys. Mater Sci Forum 638-642:1459–1463

72. Jiang B, Dong ZQ, Zhou LY, Zhang CL, Liu YZ (2016) Microstructural characterization and hardening mechanism of steel for large size bearing ring under fast heating and short soaking time condition. Steel Res Int 87(9):1127–1136. https://doi.org/10.1002/srin.201500120

73. Morito S, Saito H, Ogawa T, Furuhara T, Maki T (2005) Effect of austenite grain size on the morphology and crystallography of lath martensite in low carbon steels. ISIJ Int 45(1):91–94. https://doi.org/10.2355/isijinternational.45.91

74. Zhang CY, Wang QF, Ren JX, Li RX, Wang MZ, Zhang FC, Sun KM (2012) Effect of martensitic morphology on mechanical properties of an as-quenched and tempered 25CrMo48V steel. Mat Sci Eng A 534:339–346. https://doi.org/10.1016/j.msea.2011.11.078

75. Krauss G (1999) Martensite in steel: strength and structure. Mat Sci Eng A 273:40–57. doi:Doi https://doi.org/10.1016/S0921-5093(99)00288-9

76. Kaijalainen AJ, Suikkanen PP, Limnell TJ, Karjalainen LP, Komi JI, Porter DA (2013) Effect of austenite grain structure on the strength and toughness of direct-quenched martensite. J Alloys Compd 577:S642–S648. https://doi.org/10.1016/j.jallcom.2012.03.030

77. Koistinen DPM, E R (1959) A general equation prescribing the extent of the austenite-martensite transformation in pure iron-carbon alloys and plain carbon steels. Acta Metall 7:59–60

78. Harris WHC,M (1949) Stabilization of the austenite-martensite transformation. Trans AIME 180:447–470

79. Speich GR, Leslie WC (1972) Tempering of steel. Metall Trans 3(5):1043–1054. https://doi.org/10.1007/BF02642436

80. Kristoffersen H, Vomacka P (2001) Influence of process parameters for induction hardening on residual stresses. Mater Des 22(8):637–644. https://doi.org/10.1016/S0261-3069(01)00033-4

81. Xu DH, Kuang ZB (1996) A study on the distribution of residual stress due to surface induction hardening. J Eng Mater-T Asme 118(4):571–575. https://doi.org/10.1115/1.2805958

82. Coupard D, Palin-Luc T, Bristiel P, Ji V, Dumas C (2008) Residual stresses in surface induction hardening of steels: comparison between experiment and simulation. Mat Sci Eng A 487(1–2):328–339. https://doi.org/10.1016/j.msea.2007.10.047

83. Savaria V, Monajati H, Bridier F, Bocher P (2015) Measurement and correction of residual stress gradients in aeronautical gears after various induction surface hardening treatments. J Mater Process Technol 220:113–123. https://doi.org/10.1016/j.jmatprotec.2014.12.009

84. Holmberg J, Steuwer A, Stormvinter A, Kristoffersen H, Haakanen M, Berglund J (2016) Residual stress state in an induction hardened steel bar determined by synchrotron- and neutron diffraction compared to results from lab-XRD. Mat Sci Eng A 667:199–207. https://doi.org/10.1016/j.msea.2016.04.075